Endurecimento por precipitação

Linha Solvus

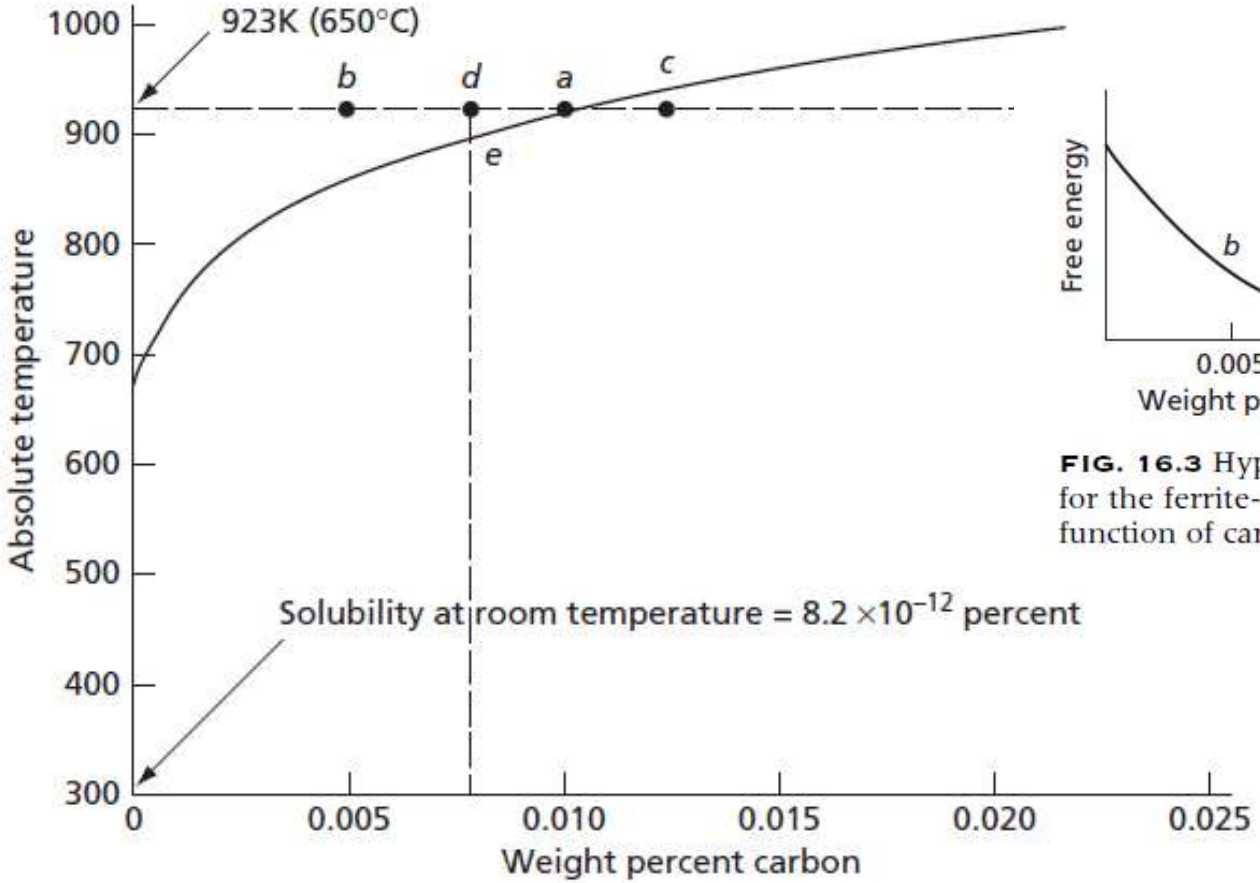

FIG. 16.1 Solubility of carbon in alpha iron

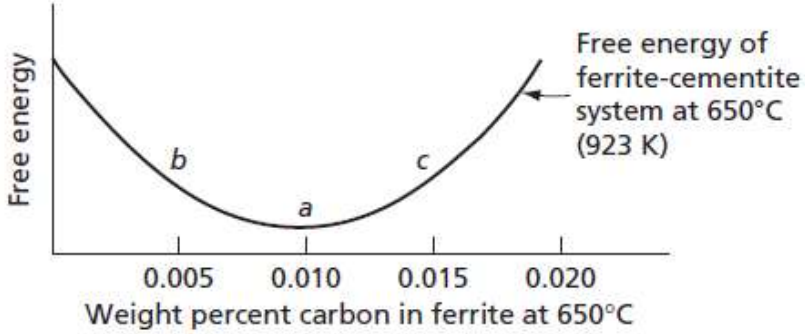

FIG. 16.3 Hypothetical free-energy curves at 600°C for the ferrite-cementite system of Fig. 16.2 as a function of carbon concentration in the ferrite

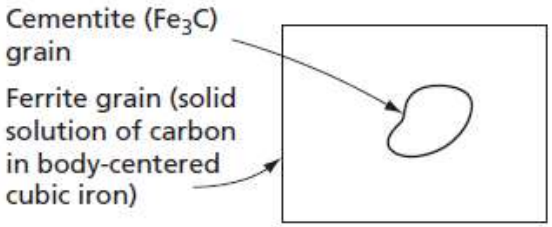

FIG. 16.2 Grain of cementite in contact with a ferrite grain

Solubilização e Envelhecimento

Al-Cu

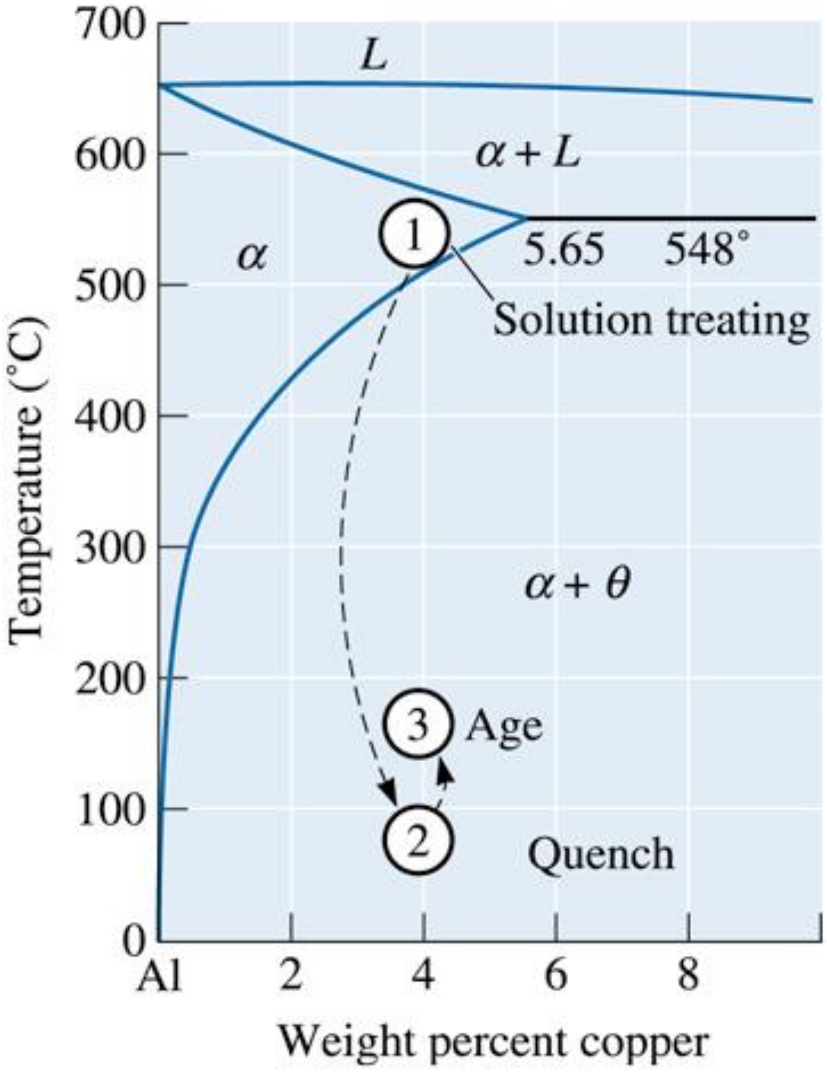

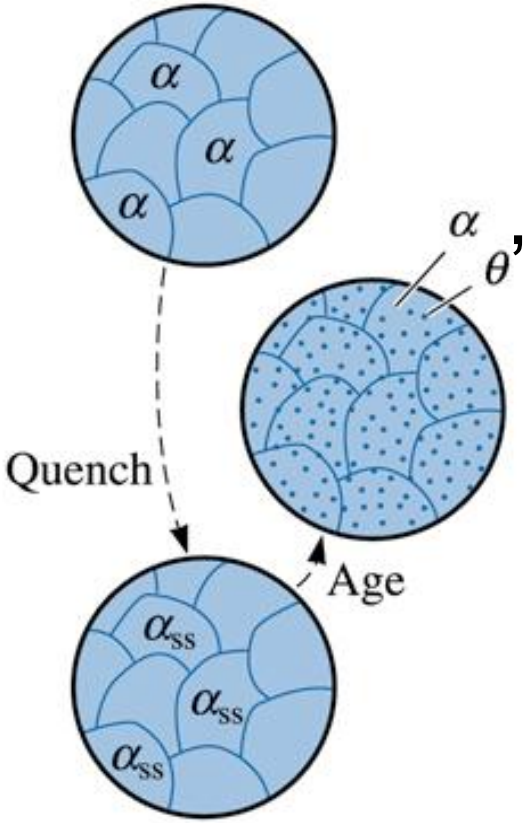

Precipitação

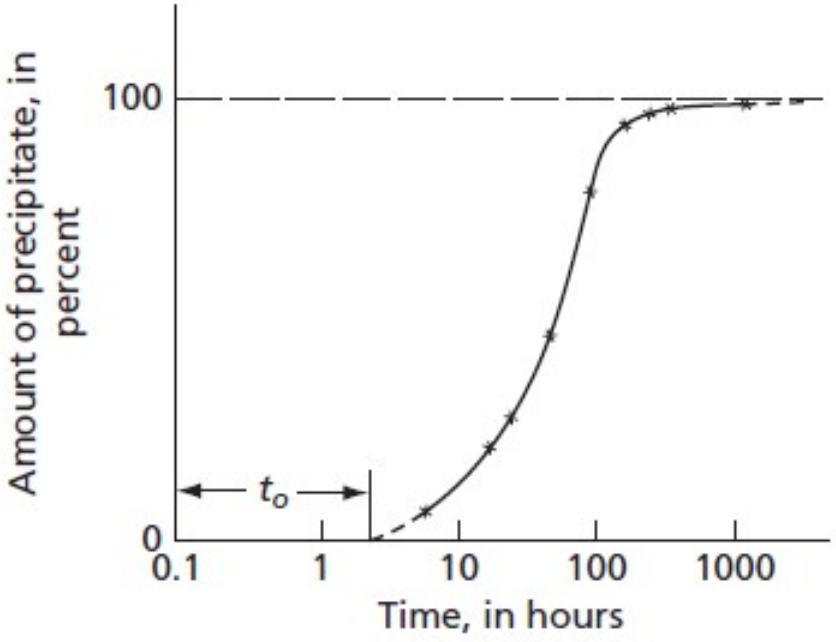

FIG. 16.4 Amount of precipitate as a function of time in an iron-carbon alloy (0.018 percent C) allowed to precipitate from a supersaturated solution at 349 K. (Data of Wert, C., ASM Seminar, *Thermodynamics in Physical Metallurgy*, 1950.)

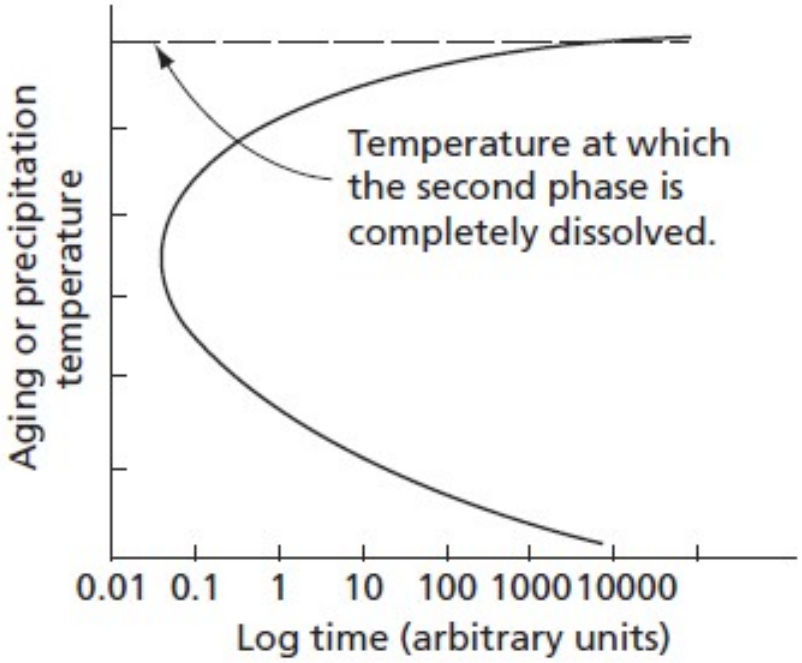

FIG. 16.5 Time for 100 percent of the precipitate to form in a supersaturated alloy

Envelhecimento

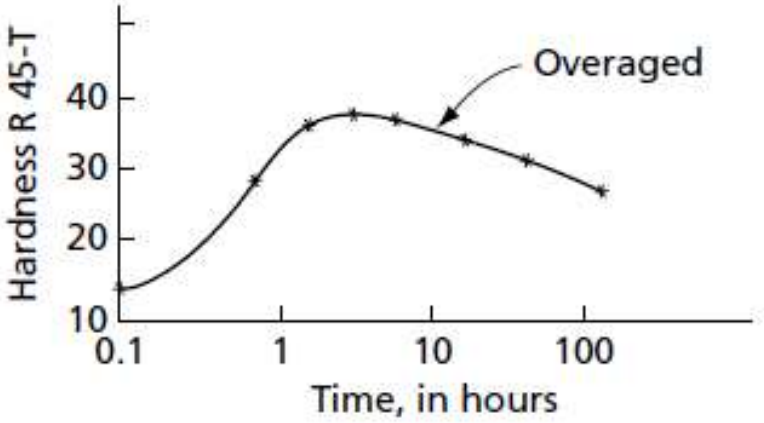

FIG. 16.6 Change in hardness during the aging treatment. Alloy is iron plus 0.015 percent C, and aging temperature 90°C. (Data from Wert, C., ASM Seminar, *Thermodynamics in Physical Metallurgy*, 1950.)

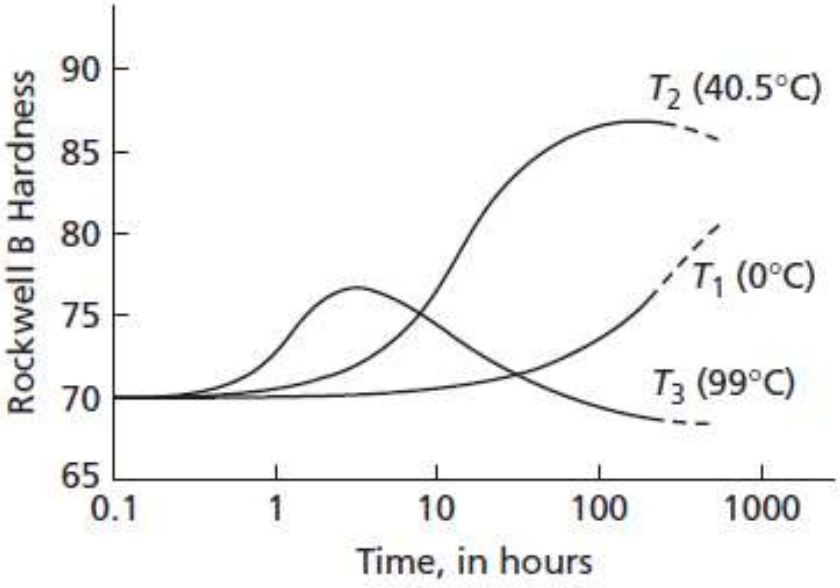

FIG. 16.7 Effect of temperature on the aging curves during precipitation hardening. Curves are for a 0.06 percent C steel. (After Davenport, E. S., and Bain, E. C., *Trans. ASM*, **23** 1047 [1935].)

Desenvolvimento dos precipitados

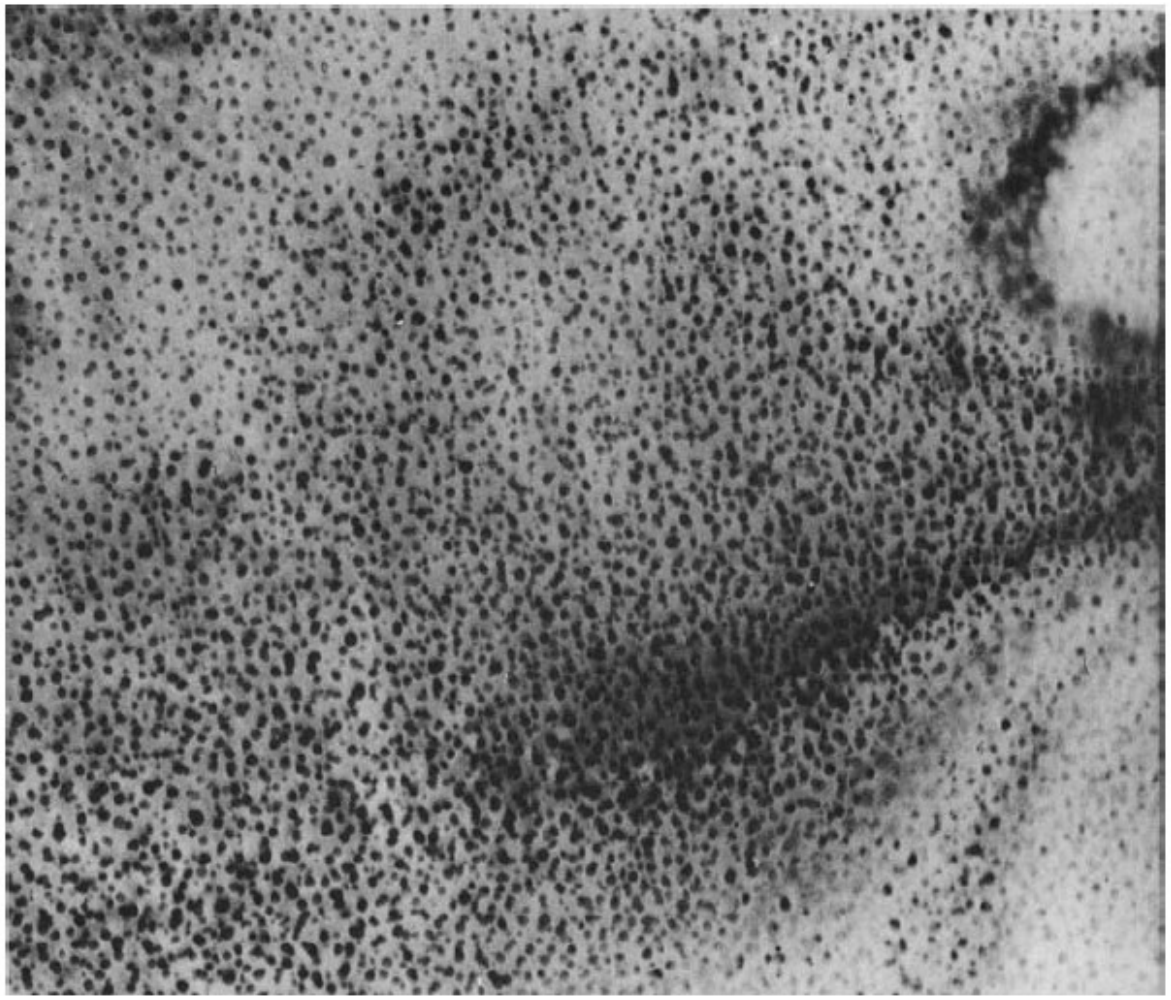

FIG. 16.8 Guinier-Preston zones in an aluminum 16 percent silver alloy. (Reprinted from Nicholson, R.B., and Nutting, J., *Acta. Met.* **9** 332 [1961] with permission of Elsevier. Photgraph courtesy of RB Nicholson. http://www.sciencedirect.com/science/journal/00016160)

Desenvolvimento dos precipitados

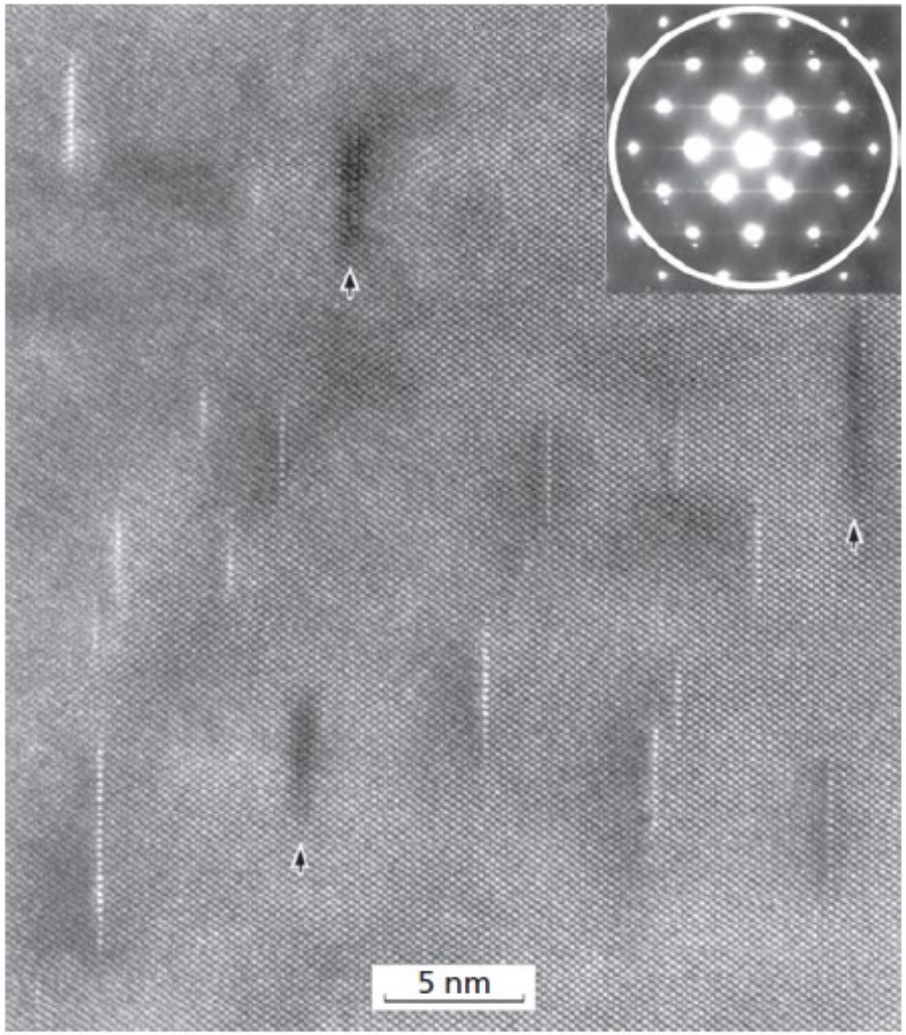

Coerentes

FIG. 16.9 GP zones in the Al-Cu 1.54 at% alloy annealed for 30 h at 100°C. The inset shows the corresponding diffraction pattern, the white circle indicating the contrast aperture position. (Reprinted from Ultramicroscopy 98, Karlik, Bigot, Jouffrey, Auger and Belliot, HREM, FIM and tomographic atom probe investigation of Guinier–Preston zones in an Al–1.54 at% Cu alloy, 219–230, Figure 1, Copyright 2004, with permission from Elsevier. http://www.sciencedirect.com/science/journal/03043991)

Desenvolvimento dos precipitados

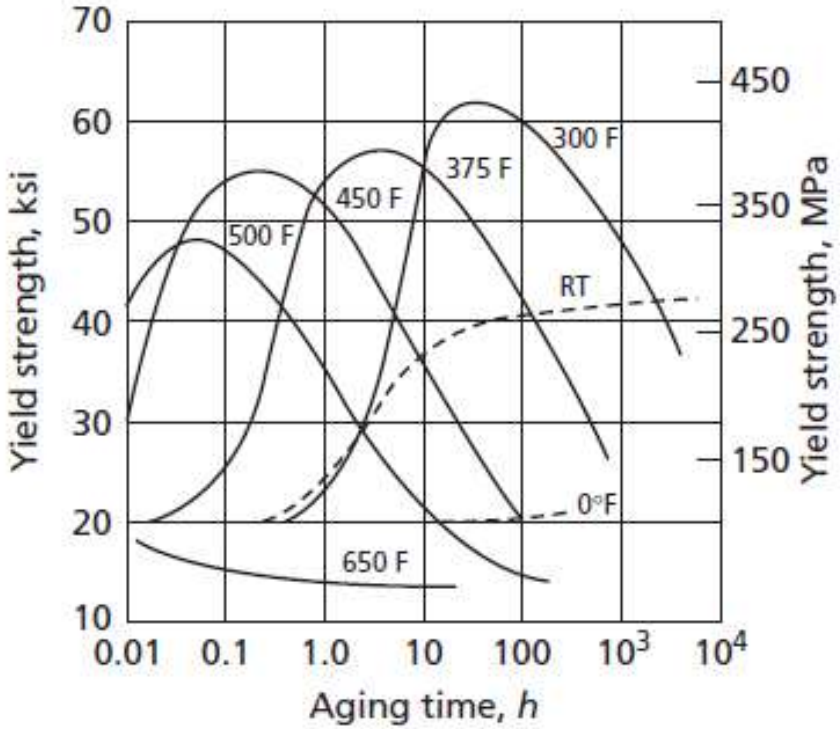

FIG. 16.10 Representative isothermal aging curves of the aluminum alloy 2014-T4. (From Hatch, J.E., Ed., *ALUMINUM Properties and Physical Metallurgy*, American Society for Metals, Metals Park, Ohio, 1984. Reprinted with permission of ASM International (R). All rights reserved. www.asminternational.org)

Desenvolvimento dos precipitados

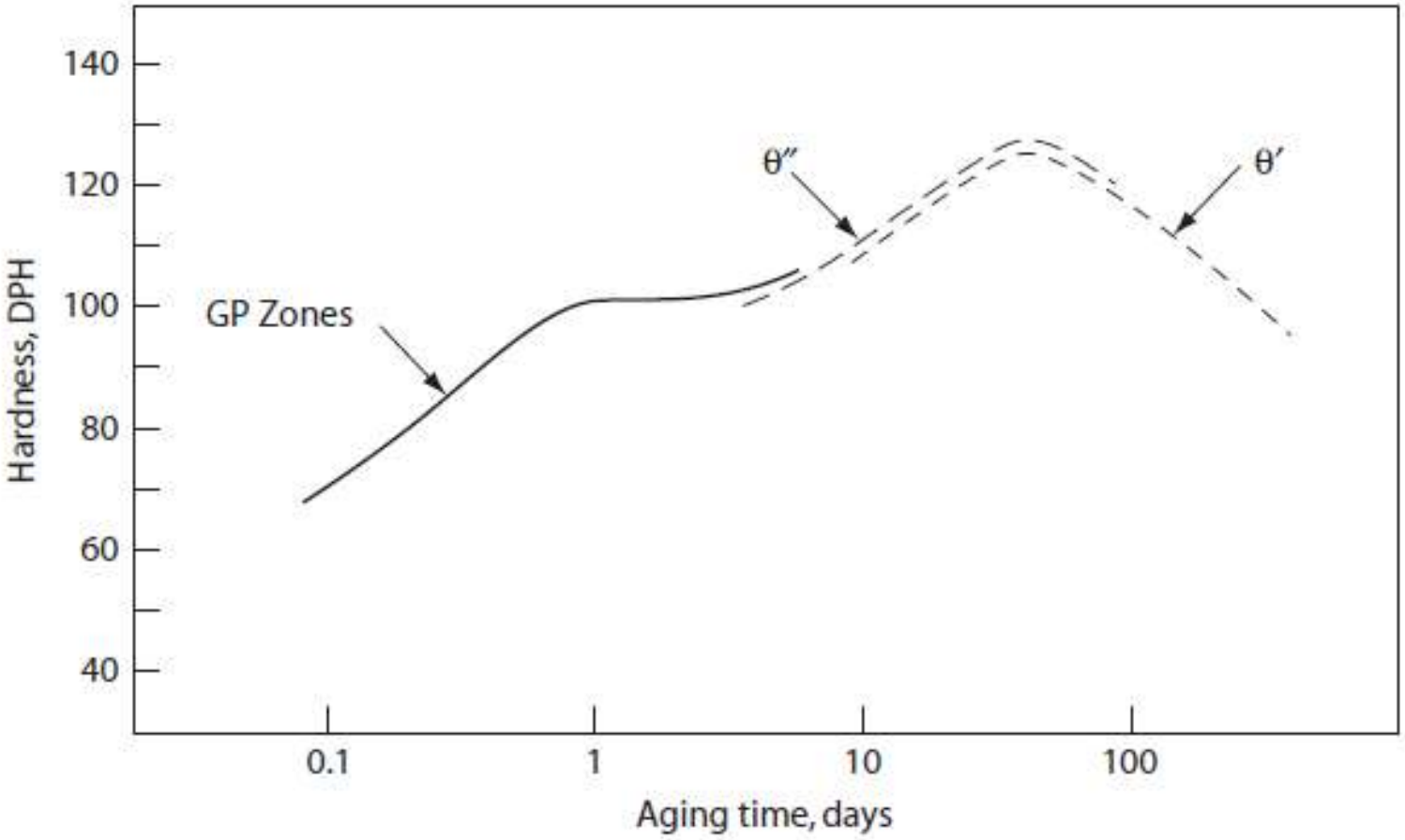

FIG. 16.11 Isothermal aging curve, Al-4 pct Cu at 130°C. (After Silcock, J. M., Heal, T. J., and Hardy, H. K., *J. Inst. Met.*, **82** 239 [1953–4].)

Precipitados coerentes e incoerentes

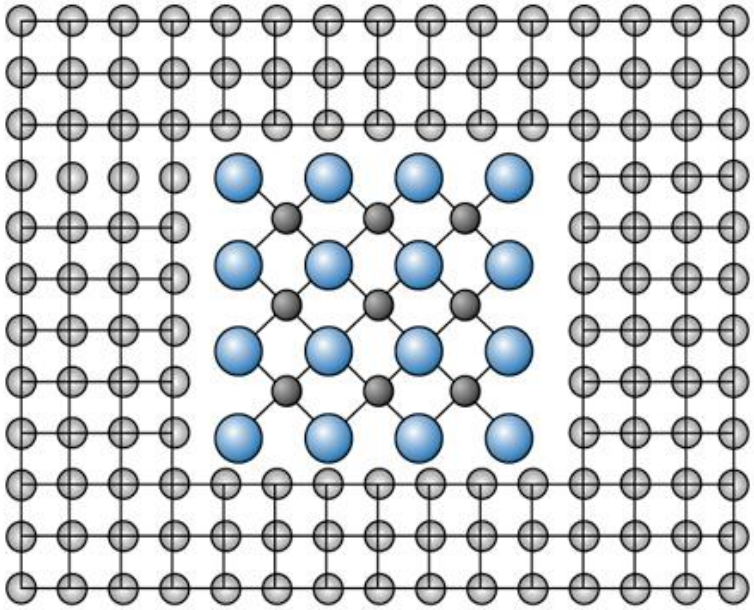

(a)

Incoerente

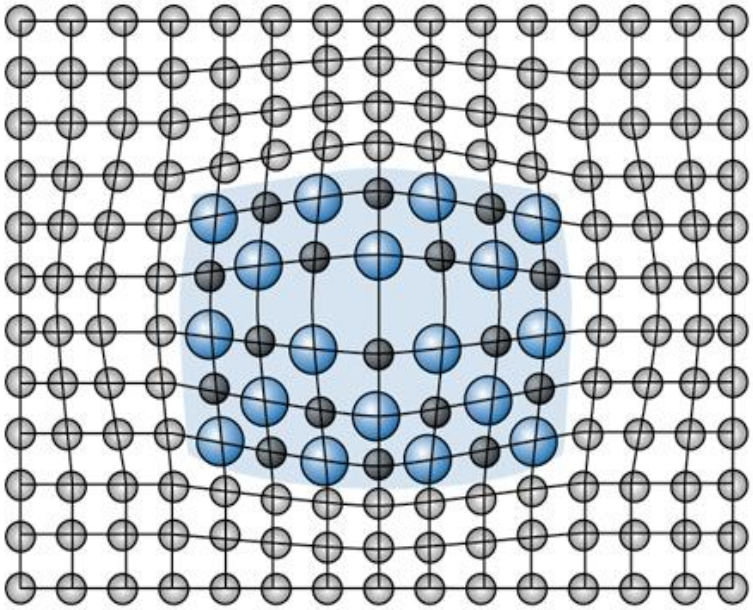

(b)

Coerente

Sequência de envelhecimento em ligas Al-Cu

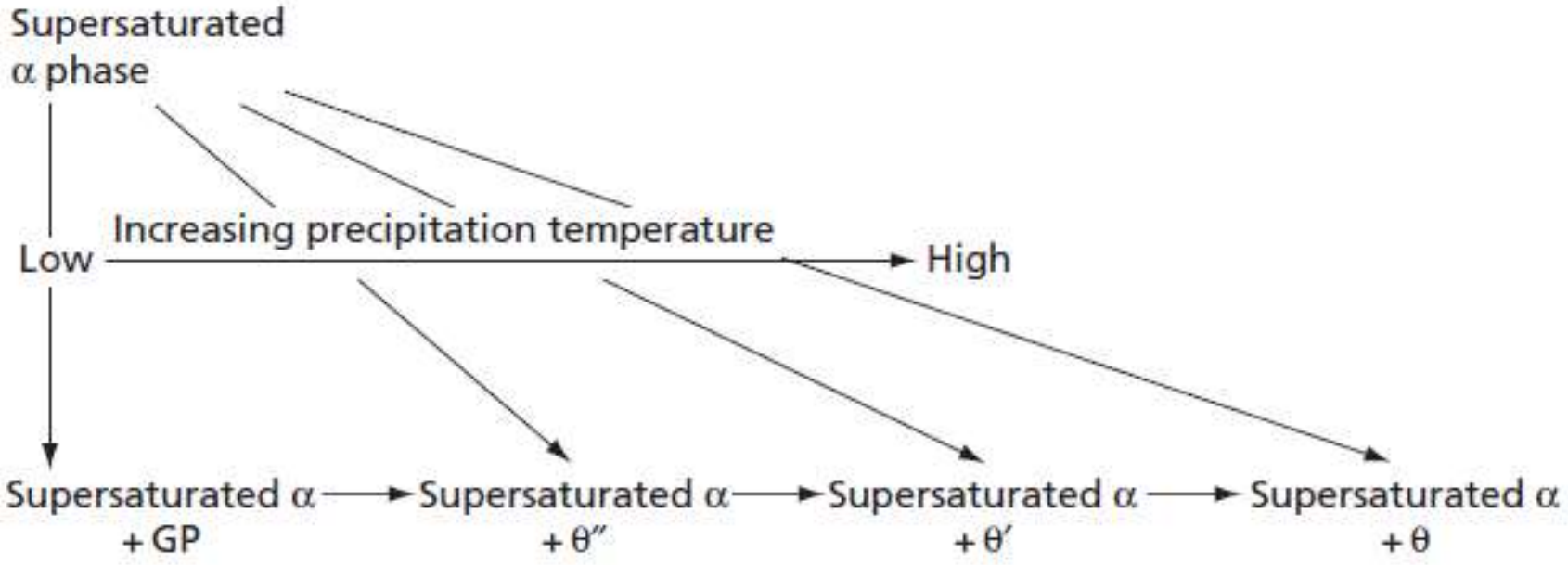

FIG. 16.12 Precipitation sequence in Al-Cu alloys

Precipitação interfásica

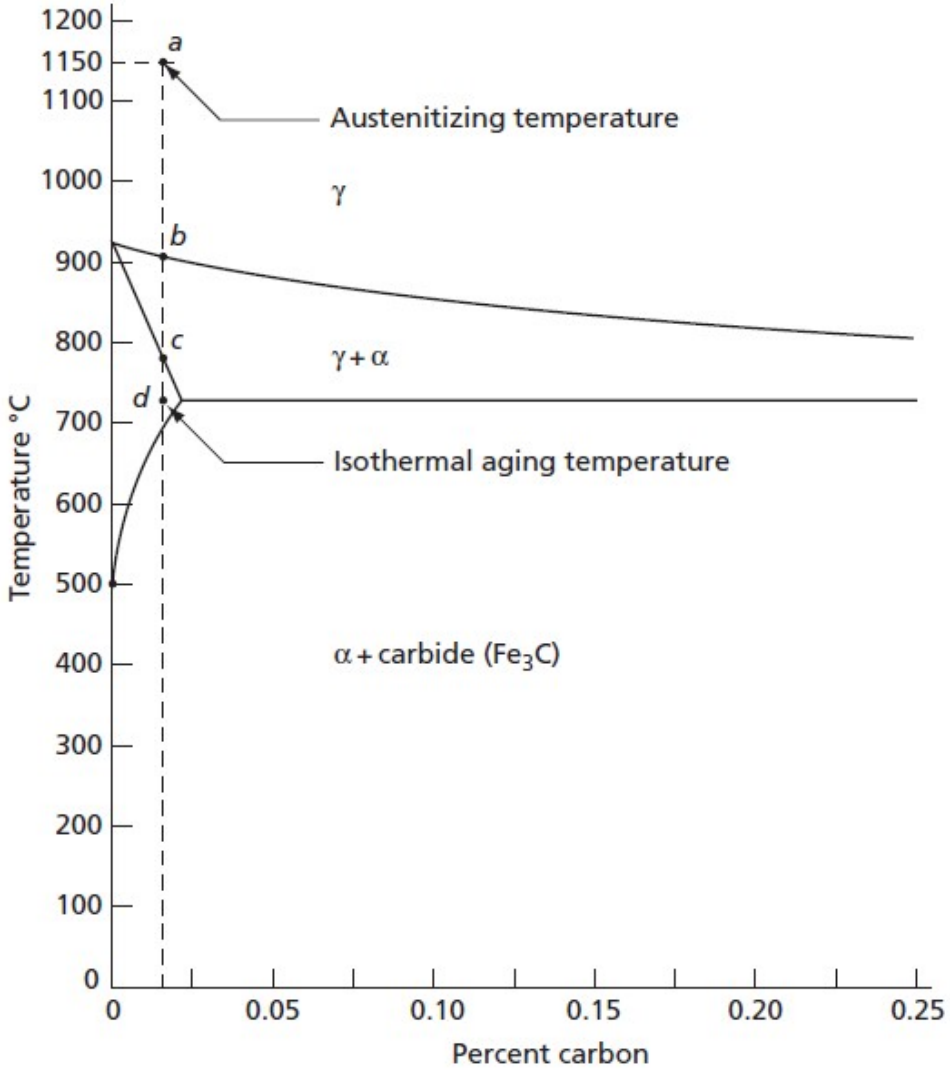

FIG. 16.15 A partial view of the iron-carbon diagram

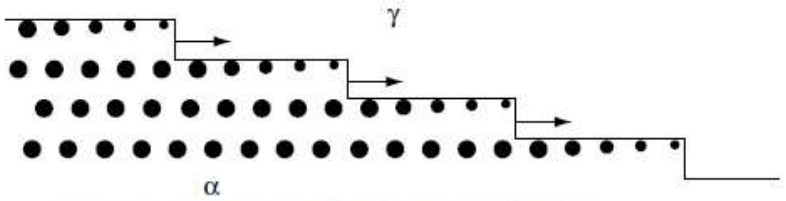

FIG. 16.16 A mechanism for the nucleation and growth of carbides on the interface between the gamma and alpha phases. (From Honeycombe, R.W.K., *Met. Trans. A* **7A** 915 [1976] with kind permission from Springer Science and Business Media.)

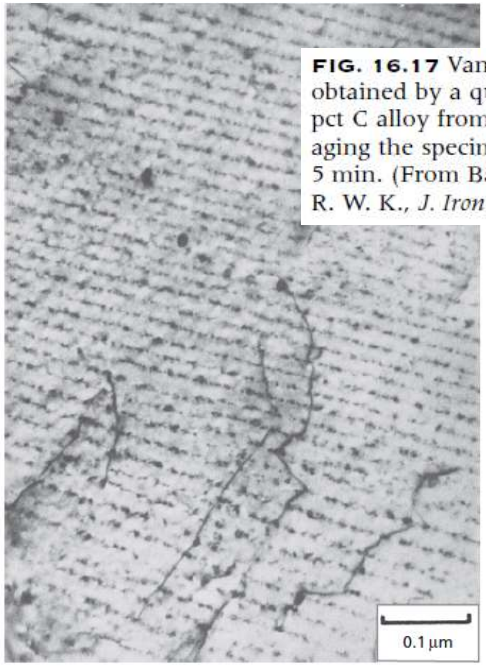

FIG. 16.17 Vanadium carbide precipitates obtained by a quench of a Fe-0.75 pct V-0.15 pct C alloy from 1150°C to 725°C and then aging the specimen at this temperature for 5 min. (From Batte, A. D., and Honeycombe, R. W. K., *J. Iron Steel Inst.*, **211** 284 [1973].)

Origem do endurecimento

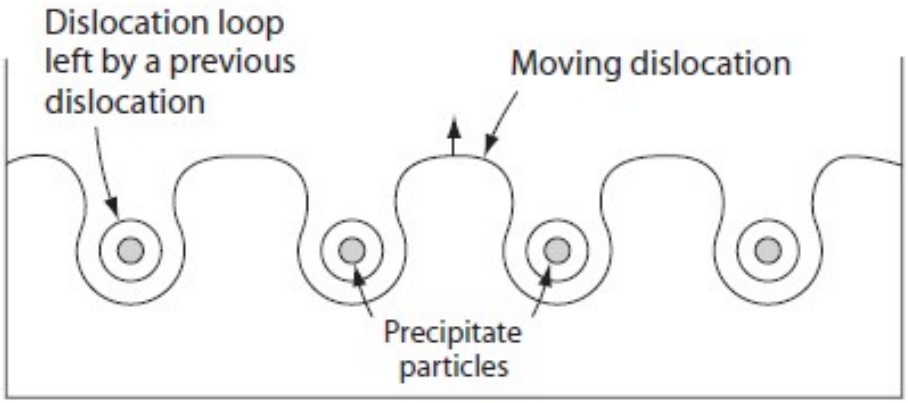

FIG. 16.18 Orowan's mechanism for the movement of dislocations through a crystal containing precipitate particles

Energia relativa ao precipitado

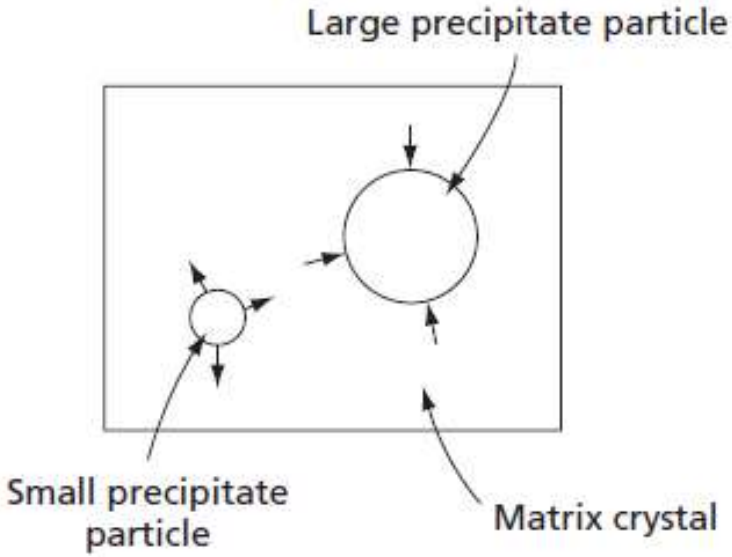

FIG. 16.19 Growth of precipitate particles. Small arrows at surfaces of particles indicate the *net* direction of the flow of solute atoms

$$\Delta G = A_1 r^3 + A_2 r^2$$

$$\Delta G' = \frac{\Delta G}{\frac{4}{3}\pi r^3} = A_1' + \frac{A_2'}{r}$$

$$A_1' = A_1/\tfrac{4}{3}\pi \qquad \text{and} \qquad A_2' = A_2/\tfrac{4}{3}\pi$$

$$\Delta G_a \approx A_1' + \frac{A_2'}{r}$$

Nucleação heterogênea

Em contornos de grão

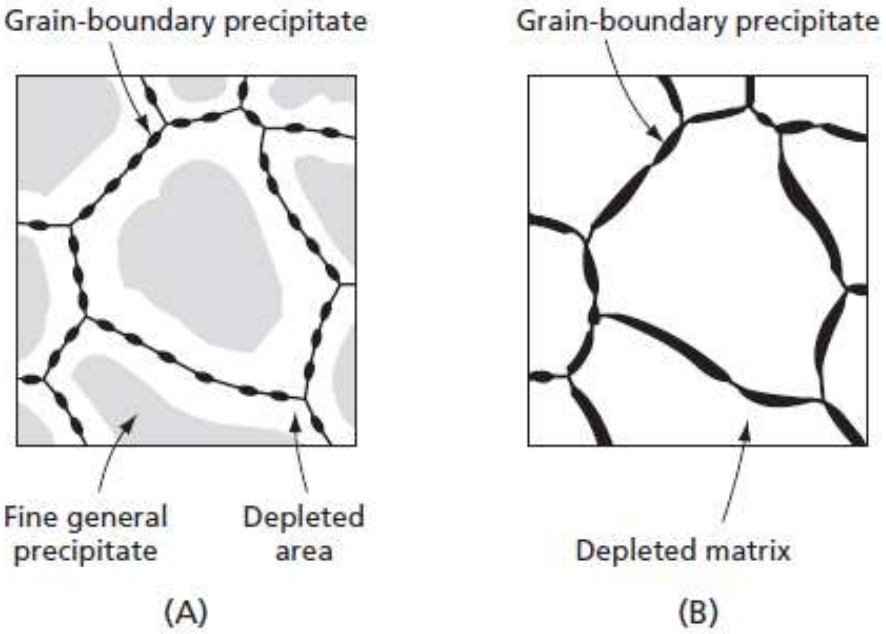

FIG. 16.20 Heterogeneous nucleation at grain boundaries. (A) Moderate rate of cooling may result in both heterogeneous nucleation at grain boundaries and homogeneous nucleation in the centers of the grains. (B) Very slow cooling may result in the precipitate occurring only at grain boundaries

Nucleação heterogênea

Em planos de escorregamento

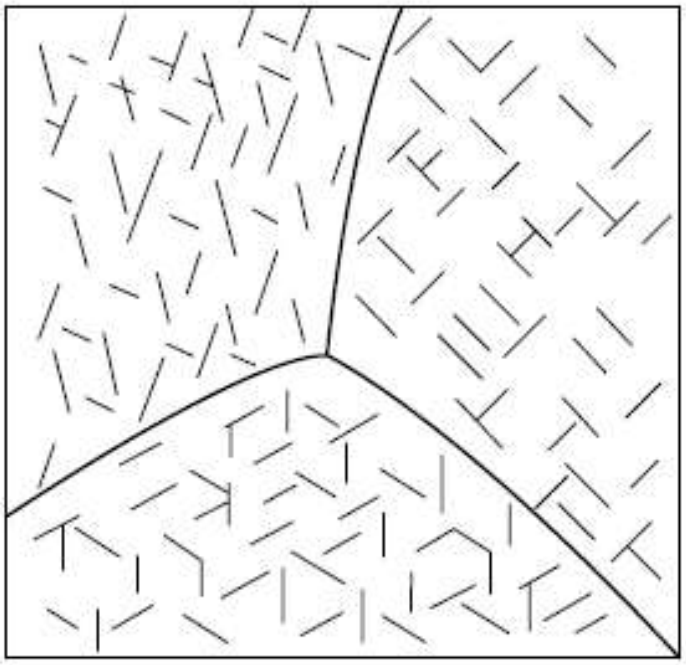

FIG. 16.21 Schematic representation of a Widmanstätten structure. Short, dark lines represent plate-shaped precipitate particles that are aligned on specific crystallographic planes of the crystals of the matrix